P2.4 DEVELOPMENT OF LONGWAVE AND WINDOW ANGULAR DISTRIBUTION MODELS FROM THE CLOUDS AND THE EARTH'S RADIANT ENERGY SYSTEM (CERES) EXPERIMENT

N. Manalo-Smith[1], N.G. Loeb[2], and K. Loukachine[3]

[1] Analytical Services and Materials, Inc., Hampton, Virginia
[2] Center for Atmospheric Sciences, Hampton University, Hampton, VA
[3] Science Applications International Corporation, Hampton, VA

1. INTRODUCTION

Earth radiation budget studies have been instrumental in enhancing our understanding of the dynamics of the Earth-atmosphere system. The radiation field emerging from a point at the top of the Earth's atmosphere (TOA) can be derived from satellite-observed radiances by applying angular distribution models (ADMs), which account for the anisotropy of the radiance field. The Clouds and the Earth's Radiant Energy System (CERES) [Wielicki et al.,1996] represents a continuing effort, set forth by its precedent, the Earth Radiation Budget Experiment (ERBE) [Barkstrom,1984, Smith et al.,1986], to produce highly accurate measurements at TOA. The CERES instrument is capable of operating in a rotating azimuth plane scan mode (RAPS) as well as in elevation in a fixed scan mode (e.g. alongtrack and crosstrack directions), thus providing multiangle radiance measurements from which ADMs can be directly determined. The CERES instrument also provides radiance measurements from three broadband channels: shortwave (0.3-5.0 μm), total (0.3-200 μm), and infrared window (8.1-11.8μm). These multiangular and multispectral measurements, coupled with cloud and aerosol properties inferred from the high-resolution spectral imager Visible Infrared Scanner (VIRS) on board the Tropical Rainfall Measuring Mission (TRMM) satellite, provides an ideal dataset for developing ADMs.

This paper gives a brief description of the development of ADMs from CERES/TRMM data and presents some results of validation studies to assess the accuracy of the empirical ADM-derived TOA LW fluxes. Eight months of CERES RAPS and alongtrack data from 40°N to 40°S are used to construct a set of ADMs for broadband longwave and window radiance fields. The ADMs are constructed by compositing radiance measurements into scene types defined by imager-derived parameters that have a strong influence on the anisotropy of the radiation field. These scene types are stratified into percentile intervals rather than discrete intervals of atmospheric and cloud parameters to ensure that each ADM scene type is adequately sampled.

* *Corresponding Author Address:* Natividad Manalo-Smith, Analytical Services and Materials, Inc. Hampton, VA 23666; e-mail: n.m.smith@larc.nasa.gov

2. THEORY AND IMPLEMENTATION

The radiance L leaving the TOA is related to the radiant flux M by the angular distribution model R:

$$L(\theta) = \frac{MR(\theta)}{\pi} \quad (1)$$

where θ is the viewing zenith angle. The emitted flux M is estimated from an instantaneous radiance measurement in a single direction if the angular distribution model is known. M is defined in terms of radiance, assuming that the outgoing longwave radiance is axisymmetric, as

$$M = 2\pi\int_0^{\frac{\pi}{2}} \sin\theta\cos\theta\bar{L}(\theta)d\theta \quad (2)$$

where $\bar{L}$ is the average radiance in the view zenith angular bin. The ADM is then computed from (1), which gives

$$R(\theta) = \frac{\pi\bar{L}(\theta)}{M} \quad (3)$$

For this study, CERES/TRMM scanner radiance measurements taken while in operation between January through August 1998 provide the dataset used to develop the broadband longwave and window ADMs. On TRMM, the CERES scene identification is based on collocated 2-km resolution VIRS measurements over a CERES footprint, which has a 10-km nadir resolution. These radiance measurements, along with scene information inferred from VIRS and meteorological parameters based on the European Centre for Medium-Range Weather Forecasts (ECMWF) data assimilation analysis, are recorded on the Single Scanner Footprint TOA/Surface Fluxes and Clouds (SSF) data product.

The radiance measurements are composited into view zenith angle ranges and scene types consisting of a combination of the underlying surface type, cloud cover, and fixed percentile intervals of atmospheric and cloud properties defined in Table 1. Under clear sky conditions, the vertical temperature change corresponds to the lapse rate in the first 300 mb of the atmosphere above the surface. For cloudy scenes, cloud infrared emissivity and the difference in temperature between the surface and cloud define the scene type. In cases of multiple layered clouds, cloud area-weighted parameter values are used. Both clear and cloudy radiation fields are also stratified by precipitable water, which is the

Cloud Category	Cloud Fraction (%)	Surface Type	Precipitable Water Percentile	Vertical Temp. Change Percentile	Cloud IR Emissivity Percentile	Total # of Scene Types
CLEAR	≤ 0.1	Ocean Land Desert	≤ 33 33 - 66 ≥ 66	$\Delta T_s < 0$ °C 0 - 25 25 - 50 50 - 75 > 75	-	45
BROKEN	0.1 - 25 25 - 50 50 - 75 75 - 99.9	Ocean Land Desert	≤ 33 33 - 66 ≥ 66	$\Delta T_c < 0$ °C 0 - 20 20 - 40 40 - 60 60 - 80 > 80	0 - 25 25 - 50 50 - 75 > 75	288 (O) 288 (L) 288 (D)
OVERCAST	≥ 99.9	ALL	≤ 33 33 - 66 ≥ 66	$\Delta T_c < 0$ °C 0 - 20 20 - 40 40 - 60 60 - 80 80 - 90 > 90	0 - 5 5 - 10 10 - 25 25 - 50 50 - 75 > 75	126

Table 1: Longwave and Window ADM Scene Types

water vapor burden from the surface to the TOA. An average radiance measurement for each combination of scene type parameters is calculated. Radiances in unsampled angular bins are estimated using a combination of theoretical model radiances and observed radiances. Using Gauss quadrature integration, the radiant flux is calculated from the mean radiances using Equation 2. The ADM is determined from Equation 3.

3. RESULTS

The ADMs and their sensitivity to the scene type parameters are illustrated in Figures 1 through 5. The ADMs are represented as a function of viewing zenith angle and in terms of an anisotropy index *AI*, which is calculated by:

$$AI = \sqrt{\frac{\sum_{i=1}^{n} (R_{ji} - R_{LAMB})^2}{n}} \quad (4)$$

where the anisotropy index gives an indication of the RMS deviation from a Lambertian case (R_{LAMB}=1) over the range of n view zenith angle bins for a scene type *j*. As the anisotropy is enhanced, the larger the anisotropy index.

Figure 1 shows that LW and WN anisotropy for a clear land scene increases as the vertical temperature change (ΔT_S) increases. The sensitivity to ΔT_S is more pronounced for the WN channel because of its larger dependence on surface temperature.

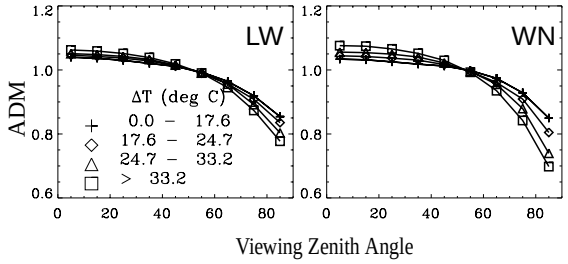

Fig. 1 Variation of Clear Sky Land (Day) with PW (33rd-66th Percentile: 1.43-2.75 cm) and ΔT_S (<25,25-50,50,75,>75 Percentile Intervals).

On the other hand, the clear ocean case (Fig. 2) show little dependence on ΔT_S. The ΔT_S has a narrower distribution over ocean than over land. The WN ADMs show slightly more limb-darkening than the LW ADMs.

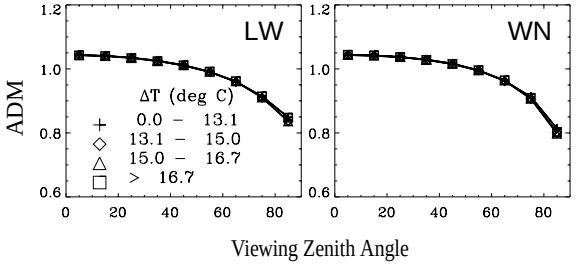

Fig. 2 Variation of Clear Sky Ocean (Day) with PW (33rd-66th Percentile: 2.29-3.48 cm) and ΔT_S (<25,25-50,50,75,>75 Percentile Intervals).

A comparison between the day and night clear-sky desert ADM anisotropic factor at nadir are shown on Figures 3a and 3b respectively. The ΔT_s intervals that correspond to each percentile interval are shown on Table 2. Daytime desert ADMs are significantly more anisotropic than the nighttime ADMs due to the differences between daytime and nighttime surface temperatures. Similarly, anisotropy increases with increasing ΔT_s for daytime since the ΔT_s range is larger for day than it is for night as shown on Table 2. Both cases show an increase with precipitable water.

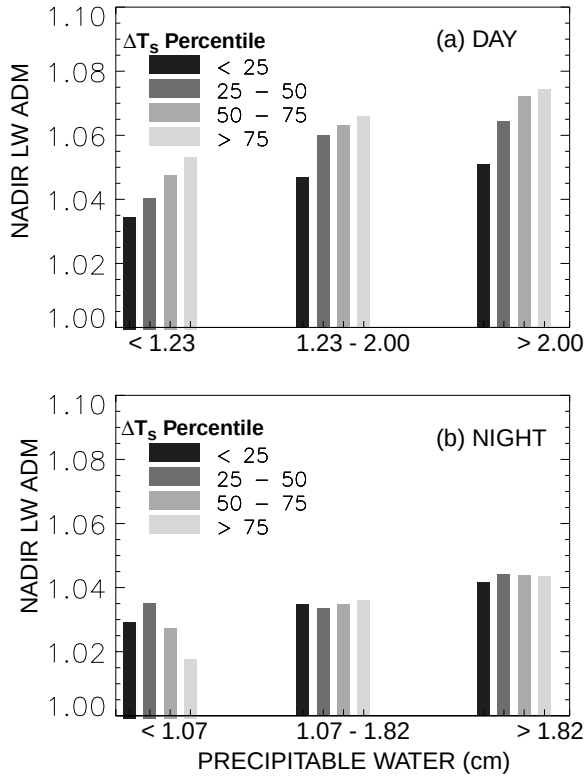

Fig. 3 Variation of Clear Sky Desert ADM (@ nadir) with PW and Vertical Temperature Change for (a) Day and (b) Night

ΔT_s %	DAYTIME			NIGHTTIME		
	PW Interval (cm)			PW Interval (cm)		
	< 1.23	1.23-2.0	> 2.0	< 1.07	1.0-1.82	> 1.82
< 25	0.0-18.8	0.0-25.5	0.0-28.7	0. -5.8	0.0-10.0	0.0 14.4
25-50	18.8-28.4	25.5-35.5	28.7- 9.1	5. 8-10.1	10.0-14.3	14.4 -18.7
50-75	28.4-38.9	35.5- 3.2	39.1-46.4	10.1-14.9	14.3- 18.9	18.7 -22.5
> 75	> 38.9	> 43.2	> 46.6	> 14.9	> 18.9	> 22.5

Table 2: Vertical Temperature Change Percentile Intervals for Clear Sky Day/Night Desert

For overcast conditions, ADMs exhibit the largest sensitivity to cloud IR emissivity. Figures 4a and 4b show the variation of overcast ADMs with ΔT_s and cloud emissivity. Anisotropy increases as the cloud emissivity decreases, particularly for thin ice clouds.

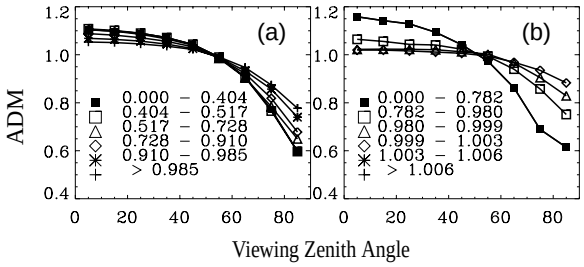

Fig. 4 Variation of Overcast Land ADM with Cloud IR Emissivity, PW (>66th Pctil: > 4.63 cm) and ΔT_s
(a) ΔT_s (20th-40th Pctil: 32.8-46.5 °C) and
(b) ΔT_s (> 90th Pctil: > 82.5 °C).

For broken cloud conditions, ADMs show the largest sensitivity to cloud cover and cloud emissivity. Figures 5a and 5b show the LW ADM index for low and high clouds, respectively over moist land regions. Anisotropy is enhanced as cloud emissivity decreases and as cloud cover and cloud height increase.

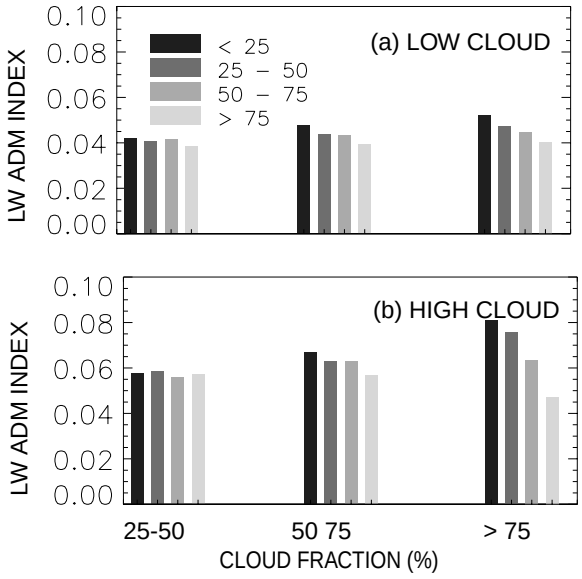

Fig. 5 LW Anisotropic Index for Broken Cloud Fields over Land (Moist Regions) vs. Cloud Fraction and Cloud IR Emissivity (a) Low Clouds (b) High Clouds

4. TOA FLUX VALIDATION

To evaluate the performance of the TRMM SSF ADMs, the TRMM ADM-derived fluxes are compared with fluxes determined by directly integrating the radiances (Eq. 2). The dependence of fluxes on viewing zenith angle is shown on Figure 6. Ideally, nadir to limb

flux should not deviate when viewing the same scene. The ERBE-like and TRMM SSF fluxes are compared to the flux computed by direct integration. For daytime, Figure 6a shows the ERBE-like all sky flux systematically decreases from nadir to limb by 3.5% (~9 W/m^2) while the CERES TRMM ADM-derived flux vary by 0.77% (~2 W/m^2) [Loukachine et al, 2002]. For nighttime, ERBE-like vary by 2.4% (~6 W/m^2) while TRMM SSF vary from nadir to limb in the order of 0.4% (~1 W/m^2).

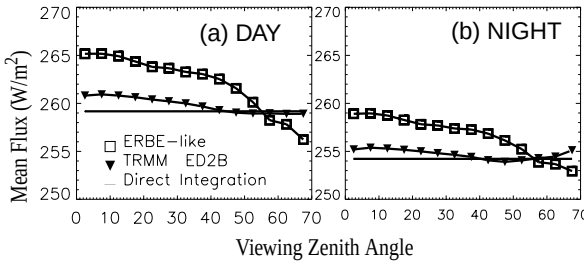

Fig. 6 All-Sky Mean LW TOA Flux (Unweighted) vs. VZA.

Another validation tool is to compare the regional (10°x10° latitude/longitude box) mean TOA flux for the TRMM and ERBE-Like fluxes with directly integrated fluxes. The flux biases are weighted to account for the relative effects of viewing zenith angle on gridded time-averaged fluxes [Young et al., 1998]. The zonal bias plots (Figures 7 and 8) show that when only footprints within $\theta < 50°$ are used, the zonal mean ERBE-Like flux bias reaches values of up to 5 W/m^2 but is reduced significantly for $\theta < 70°$. CERES TRMM zonal biases are consistently in the order of < 1 W/m^2 for $\theta < 70°$. Table 3 summarizes the global mean bias and RMS errors.

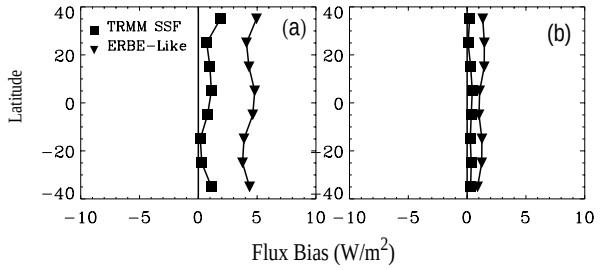

Fig. 7 Daytime Mean LW Flux Zonal Bias for (a) $\theta < 50°$ and (b) $\theta < 70°$.

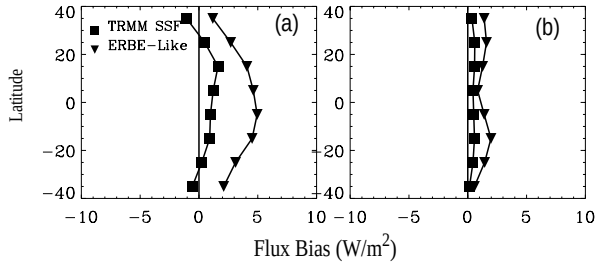

Fig. 8 Nighttime Mean LW Flux Zonal Bias for (a) $\theta < 50°$ and (b) $\theta < 70°$.

θ-range	ERBE-Like				CERES/TRMM			
	DAY		NIGHT		DAY		NIGHT	
	Δ	σ_Δ	Δ	σ_Δ	Δ	σ_Δ	Δ	σ_Δ
$\theta < 50$	4.35	4.60	3.50	3.97	0.87	1.62	0.54	1.43
$\theta < 70$	1.22	1.33	1.32	1.49	0.29	0.49	0.46	0.58

Table 3: Monthly mean regional LW TOA flux bias and RMS error for ERBE-Like and TRMM SSF.

5. SUMMARY

Angular Distribution Models (ADMs) for broadband LW and WN (8.1-11.8 μm) regions were developed using CERES TRMM multiangle radiance observations concurrently with scene information from the high-resolution VIRS imager. CERES ADM-derived fluxes showed less dependence on viewing geometry (~0.77%) compared to the systematic decrease from nadir to limb of ~3.5% for ERBE-Like fluxes. Regional TOA flux accuracy improved by a factor of 3 compared to ERBE.

6. REFERENCES

Barkstrom, B.R. 1984: The Earth Radiation Budget Experiment (ERBE), Bull. Amer. Meteor. Soc, 65, 1170-1186.

Loeb, N.G., N. Manalo-Smith, K. Loukachine, S. Kato, and B. A. Wielicki, 2002: A new generation of angular distribution models for top-of-atmosphere radiative flux estimation from the Clouds and the Earth's Radiant Energy System (CERES) satellite instrument, *11th Conference on Atmospheric Radiation*, Ogden, Utah.

Loukachine, K., N.G. Loeb and N. Manalo-Smith, 2002: Validation of top-of-atmosphere radiative flux estimates from the Clouds and the Earth's Radiant Energy System (CERES) Angular Distribution Models, *11th Conference on Atmospheric Radiation*, Ogden, Utah.

Smith, G.L., R.N. Green, E. Raschke, L.M. Avis, J.T. Suttles, B.A. Wielicki, and R. Davies, 1986: Inversion Methods for Satellite Studies of the Earth's Radiation Budget: Development of Algorithms for the ERBE mission, Rev. Geophys., 24, No.2, 407-421.

Wielicki, B.A., B.R. Barkstrom, E.F. Harrison, R.B. Lee III, G.L.Smith, and J.E.Cooper,1996: Clouds and Earth's Radiant Energy System (CERES): An Earth Observing System experiment, Bull. Amer. Meteor. Soc., 77, 853-868.

Young, D.F. et al., 1998: Temporal interpolation methods for the Clouds and the Earth's Radiant Energy System (CERES) experiment, *J. Appl. Meteor.*, 37,572-590.